# Chaos in a Driven Mechanical Oscillator

Carson Bullock
*Department of Physics, The College of Wooster, Wooster, Ohio 44691, USA*
(Dated: 7 May, 2018)

A forced, damped, nonlinear oscillator was shown to exhibit chaotic behavior at driving frequencies slightly below its resonant frequency. Phase space diagrams that lack periodicity and show sensitivity to initial conditions are contrasted with phase spaces in a periodic regime. Potential wells were calculated, showing that the Duffing oscillator is bistable, regardless of whether its regime is chaotic or periodic, but that the symmetry of the potential well is contingent upon whether the springs used have equal stiffness. The full range of motion of the system, additionally including the angle of the driver, is presented in cylindrical coordinates.

## INTRODUCTION

In 1918, Georg Duffing published analyses of oscillatory behavior and resonance in systems that had not been previously studied [1]. The Duffing oscillator is an example of a forced, damped, nonlinear oscillator. To unpack these qualities, forced refers to the fact that the oscillator is driven with a constant frequency $\omega_{\mathrm{d}}$, while damped refers to a gradual decay in motion due to damping forces like internal friction and air resistance that oppose velocity. In a driven, damped, *harmonic* oscillator, the system has two qualitatively different stages, a transient regime dominated by initial conditions and a steady state regime dominated by the driver parameters as the transient motion dies down [2, 3]. In these harmonic systems, the potential well characterizing the system is parabolic, with only one stable equilibrium point at zero displacement, and potential energy increases with increasing displacement. However, in the Duffing oscillator, the potential well has two stable equilibria equally spaced from a central unstable equilibrium, which gives rise to very different motion. The Duffing oscillator can be made to undergo a transient regime and a steady driver-dominated regime, but it could be alternatively made to undergo chaotic motion. Chaotic systems are patterned but non-repeating, and are extremely sensitive to slight differences in initial conditions.

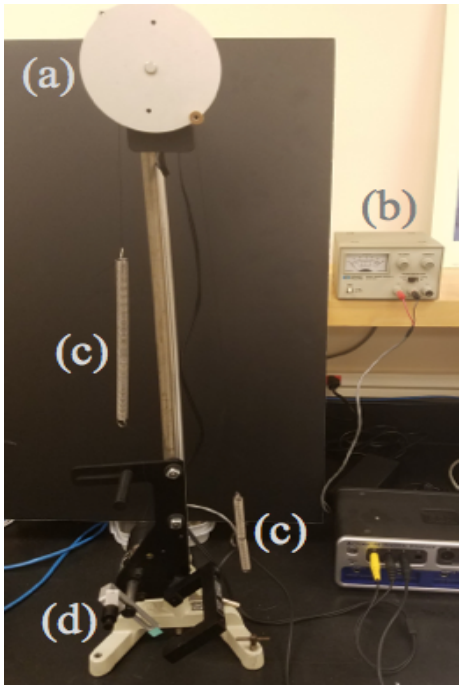


FIG. 1: Components of the apparatus pictures as follows: (a) rotary motion sensor wheel to which the springs are attached; (b) two springs; (c) the voltage generator to power the motor; (d) the driving arm, motor and photogate.

## THEORY

An ideal single spring is subject to Hooke's Law,

$$F = -k(x - x_0) \, , \tag{1}$$

such that the magnitude of the restoring force, based on the stiffness constant $k$, increases the further a spring is stretched or compressed from its equilibrium position $x_0$. By Newton's Second Law

$$\ddot{x} = \left(\frac{-k}{m}\right) x \, , \tag{2}$$

where here we have redefined $x$ as a shorthand for the displacement. Solutions to this equation are sinusoidal, which fits the understanding that the velocity will be maximized when the displacement is zero, and vice versa. Suppose then, that Hooke's Law does not totally apply, and instead there is an additional nonlinear term. Materials may not be ideally Hookean for a variety of reasons, for example, if the stiffness is stress or temperature dependent. With the inclusion of this nonlinear term, a corresponding strength coefficient $\beta$, and the redefinition of $k/m = \omega_0^2$, we have

$$\ddot{x} = -\omega_0^2 x - \beta x \, . \tag{3}$$

This equation would only hold for an object in a vacuum, because otherwise air resistance will provide damping. Quadratic drag is applicable to situations of relatively high speeds and large cross-sectional areas, so I will dis-

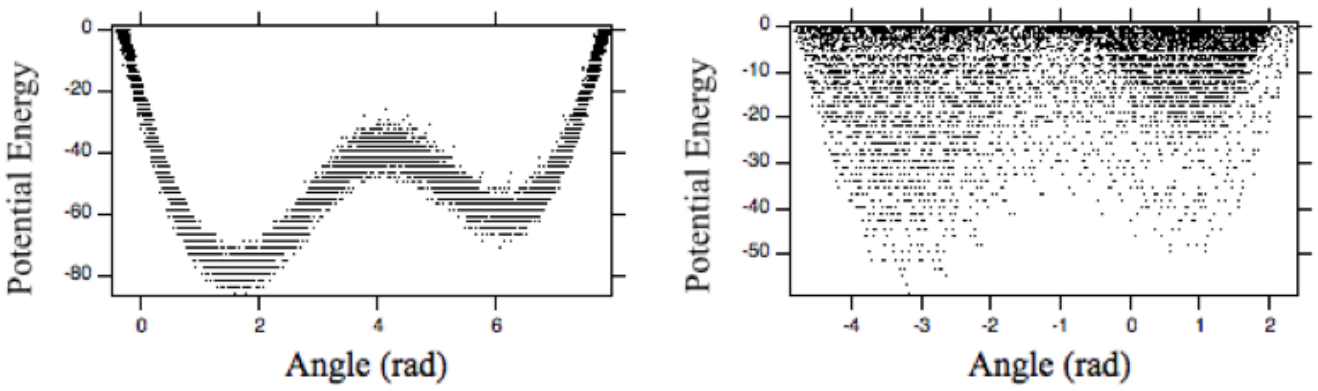


(a) (b)

FIG. 2: Potential energy vs. angular displacement plots for (a) periodic and (b) chaotic data. Total energy is set at zero, such that at the top of the plot, all energy is potential and thus none is kinetic. The points for the periodic regime trace out the outline of the well, while the chaotic regime shows that points may be found anywhere within the well with varying likelihoods. Horizontal bands are artifacts caused by the limited precision of measurement.

count it because the springs and wheel are small and traveling relatively slowly, but that still leaves a linear drag term, proportional to the velocity. We now have

$$\ddot{x} = -\omega_0^2 x - \beta x - \delta \dot{x} \ , \tag{4}$$

wherein the drag force opposes the direction of motion, so this term is also negative. So far, I have derived the equation of motion for a damped, nonlinear oscillator, but to model the Duffing equation there must be a final driver term. If this driver is sinusoidal, with an amplitude $\gamma$ and a frequency $\omega_d$, we can move the prior terms to the other side to obtain

$$\ddot{x} + \delta \dot{x} + \omega_0^2 x + \beta x = \gamma \sin(\omega_d t) \ , \tag{5}$$

the full second-order differential equation used by Duffing.

The search for an analytic solution is outside of the scope of this analysis. One might nevertheless look for ways to reduce this form into something more manageable. When two simple harmonic oscillators are coupled, the resulting motion gains unique properties. The motion of two coupled oscillators can be decomposed into two normal modes, generally an in-phase and anti-phase mode. Any observed motion can be written as a linear combination of these two normal modes, representing a superposition. In the language of linear algebra, it can be equivalently stated that any $n$ linearly independent vectors will form a basis for $\mathbb{R}^n$ and span the plane, where here the vectors are our two normal modes and $\mathbb{R}^2$ can be considered the space of all position-velocity pairs. This principle applies to both free and forced oscillation. However, the leap from linear motion to the nonlinear dynamics in the Duffing oscillator require reconceptualizing the notion of normal modes. Kerschen *et al.* lay out several key reasons why normal modes have not historically been considered an important tool in nonlinear analysis [4], a few of which I will adapt here:

1. Nonlinear systems' range of behavior is far wider and more complex than linear systems, including behaviors present in the Duffing system like bifurcations, limit cycles, and chaos.

2. Superposition, which underlies the usefulness of normal modes to linear systems, is not applicable to nonlinear systems.

Kerschen *et al.* also highlight that analyses of nonlinear normal modes have also been limited to low-order systems, a drawback which is not relevant here because the Duffing equation is only second-order. For these reasons, normal modes are not nearly as applicable to the Duffing oscillator as they are to the linear case, so it is not easily reducible.

## APPARATUS AND PROCEDURE

A prebuilt PASCO apparatus, consisting of two springs connected via a rotary motion sensor wheel, is displayed in Fig. 1. Power is supplied to a motor, which turns a lever arm attached to one of the springs. This spinning arm is a sinusoidal oscillator. The frequency of the driver was not directly under my control, rather, I changed the voltage input to the motor, and voltage was found to be roughly proportional to frequency. A photogate marks when the driver passes a certain angle, simply outputting a blocked or unblocked status. Raw data were transferred from the apparatus for analysis through PASCO's Capstone data collection software. Trials lasted between 5 and 15 minutes, with data resolutions of 40 points recorded per second. Because the Capstone interface is

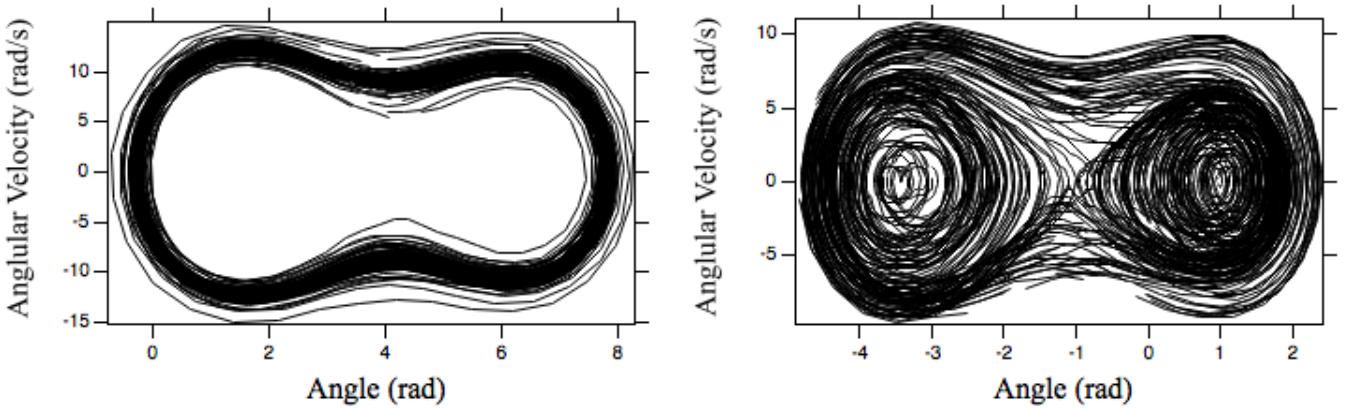


(a) (b)

FIG. 3: Full phase space graphs from (a) a periodic trial and (b) a chaotic trial over similar timescales. Periodic conditions are characterized by high system energy, corresponding to a driver frequency of approximately $\omega_d = 4.1$ rad s$^{-1}$, while chaos is observed at a lower frequency, approximately $\omega_d = 3.9$ rad s$^{-1}$. Points that occurred sequentially in time are connected by a line. In (a), the motion initially wobbles before settling into a steady periodic regime, while in (b) the motion does not repeat itself, even after long time periods.

unable to simultaneously receive inputs from both the rotary motion sensor and the photogate, slight data massaging is necessary to properly align the photogate data with the corresponding angle and angular velocity data.

By assuming that total energy is zero, it follows that

$$U = -K = -\frac{mv^2}{2} , \tag{6}$$

and thus we are able to generate a well of the potential energy $U$ by graphing the negative kinetic energy $K$. Thus, Fig. 2 shows the square of the velocity vs. the angular displacement. The spring constants, $k_1$ and $k_2$, are unknown, but they cannot be assumed to be approximately equal, because the two sides of the wells in Fig. 2 are asymmetric. While the apparatus was originally billed as symmetric [5], this observed asymmetry could be because the spring on the right of Fig. 1 is visibly deformed, and this bend could be responsible for altering the strength of its restoring force.

## RESULTS

The natural frequency of the system was found to be near $\omega_0 = 4.2$ rad s$^{-1}$ because it resonates when the driver has a period of $T = 2\pi\omega_d^{-1} = 1.5$s. Closely related, the scope of the parameters available for experimentation was limited. Driving frequencies below about $\omega_d = 3.5$ rad s$^{-1}$ and above $\omega_d = 4.8$ rad s$^{-1}$ (periods of 1.82 s and 1.31 s, respectively) were insufficient to maintain long-term motion. The wheel lost energy due to incompatibility between the driver frequency and natural frequency of the springs, and quickly became unable to transition from one stable equilibrium to the other. This low energy state would be represented graphically as if the dumbbell in Fig. 3(a) was cut in half. Frequencies at exactly 4.2 rad s$^{-1}$ were also unsustainable for practical reasons due to resonance, as the springs gained too much energy and bounced loose from the grooves on the sensor wheel. The experimental variable used to generate the stark differences between periodic and chaotic regimes was driver frequency. The nearer the driving frequency was to the natural frequency of the springs, the higher the energy level was in the system, ensuring that the wheel always had enough energy to crest the unstable equilibrium at the center of Figs. 2(a) and (b). When the energy was lowered even further from the maximum, by increasing or decreasing the driving frequency further from resonance, chaos could be observed within a critical range of driving frequencies.

Plots of angular velocity of the wheel vs. angle of the wheel are given in Fig. 3. An attractor is a stable set of points toward which a system evolves after repeated iteration. For the periodic regime in Fig. 3(a), the thickest inner loop of the dumbbell shape is a standard attractor: a set of points on the coordinate plane to which the system is drawn in. Fig. 3(b) also depicts an attractor, but due to its highly detailed structure it is known as a *strange* attractor. Provided that data were taken with high enough precision over a long enough duration, one could look at a portion of the image that had been arbitrarily enlarged and still see the same level of fine detail. In this context, the chaotic regime of the Duffing oscillator can be considered a fractal in that it has a dimension that is not a whole number. Rather, prior research has found the phase space to be roughly 1.4-dimensional [6]. My data do not have the requisite precision to verify this fractal dimension because the data were rounded by Capstone.

The phase space plots in Fig. 3 include points taken at

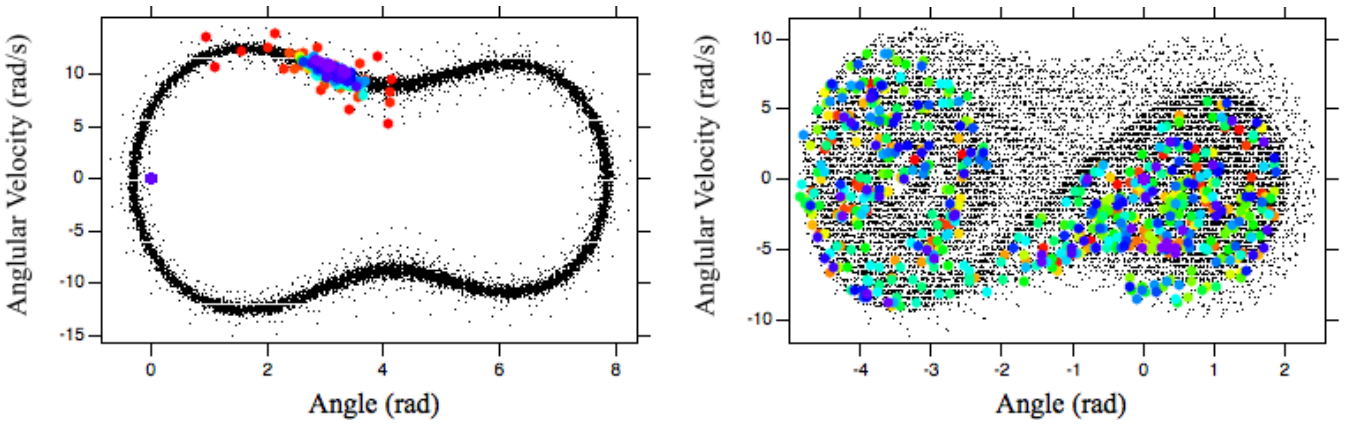


(a) (b)

FIG. 4: Poincaré plots for (a) periodic and (b) chaotic conditions. To transition from (a) to (b) the driver frequency was lowered, thereby reducing resonance and producing chaos because the sensor wheel only had enough energy to transition between the equilibria points some of the time. Hexagonal markers show a subset of the data for a specific driver angle, colored by time, while black dots in background show the full data, measured at all other driver angles.

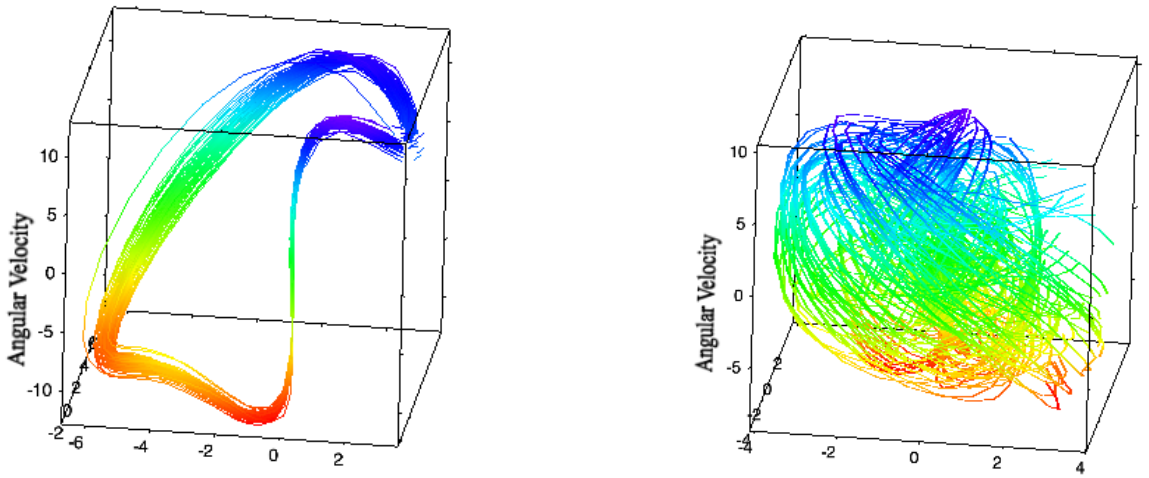


(a) (b)

FIG. 5: Poincaré sections distributed radially according the the angle of the driving arm for (a) periodic and (b) chaotic conditions. Again, the driving frequency is closer to the resonance in (a), and unlike (b) it is able to freely and consistently transition between equilibria. A singular path is formed in (a) due to the low spread seen in Fig. 4(a). In other words the phase space data are constant for a given driver angle. Conversely, in chaos, the phase space data are highly varied at any given driver angle, thus any individual section appears jumbled and their radial distribution in (b) appears like a ball of twine. In both (a) and (b), points are colored by their $z$-position, with red being lowest and purple being highest, to provide a sense of depth.

every angle of the driver arm. If we select for certain angles, for example by excluding all points except when the driver arm is parallel with the ground, we will produce a Poincaré section. This is shown in Fig. 4 by the colored dots, displayed on top of the full data in black. We can see in Fig. 4 that when the oscillator is in a periodic regime the section repeats itself, while the points are distributed chaotically in the aperiodic regime. In Fig. 4(a), red hexagons give begin with a spread around the top-left region, and over time hone in on the section covered by dense purple hexagons, indicating an increase in periodicity of the phase space. Conversely, in Fig. 4(b), no

such increase in periodicity can be seen, as the colored markers are equally spread out at the beginning of the trial as it is at the end.Because each driver angle will produce a different Poincaré section, the Poincaré sections for every angle of the driver from zero to $2\pi$ could all be stacked atop one another to recreate the full phase space diagram in Fig 3.

Finally, I synthesized the data shown above into one cohesive plot. Using cylindrical coordinates where driver angle is graphed in $\phi$, wheel angle is graphed in $r$, and wheel angular velocity is graphed in $z$, we obtain the three-dimensional path plotted in Fig. 5, appearing like a ball of twine wound around the $z$-axis. Because the angular velocity of the driver arm is constant in time, the path travels around the $z$-axis at a constant azimuthal velocity, but moves freely in the $r$- and $z$- axes, like a game of tether ball. Any radial cross-section, by which I mean any planar cut from the $z$-axis outward, will produce a Poincaré section similar to the colored markers in Fig 4, cycling continuously through all sections before repeating. While the $r$- and $z$-axis data were measured experimentally, the $\phi$ coordinate data were generated based on the driver period. This period is not perfectly consistent throughout time, so the point at which the photogate was triggered was always assigned an angle of zero radians, and then the remaining $2\pi$ radians were divided evenly between however many points were taken until the photogate was triggered again.

## CONCLUSIONS

I have successfully derived the Duffing equation, seen in Eq. (5), and have graphically shown a set of possible solutions given fixed parameters like the spring constants and the viscosity of the air. These solutions can be either periodic or chaotic. Periodic regimes are observed as a result of resonance, when the driving frequency is very close to the natural frequency of the oscillator, because in this state the energy of the system is high, and the wheel is always able to transition between the equilibria of the potential well. Conversely, chaos is observed when the energy of the system is slightly lower, and the motion sensor wheel can usually, but *not* always transition between stable equilibria. At even lower energies, the system can again be considered trivially periodic, because it will be stuck in one of the sides of the well, never able to transition. These qualitative differences have been made clear through numerous graphical comparisons.

This experiment did not change any of the fundamental parameters of the apparatus, such as the spring constants or the viscosity of the environment. Further experimentation could alter these parameters to observe new phase space plots. It is known that parameters exist such that a period-doubling route to chaos, one in which the periodicity doubles at increasingly short intervals, could be observed if the amplitude of the driver is used as the independent variable rather than driving frequency. Likewise, I paid little heed to the effects of the magnetic damper that came included with the PASCO apparatus, and further experimentation could include this second damping term in the equation derivation.

## ACKNOWLEDGMENTS

Thanks goes to Hwan Michelle Bae for writing cogent instructions on unintuitive parts of the procedure and for her willingness to share her experience.

[1] Duffing, Georg. “Erzwungene Schwingungen bei vernderlicher Eigenfrequenz und ihre technische.” *Journal of Applied Mathematics and Mechanics.* 1(1) (1921).
[2] Gilchrist, Alexei. “Driven and Damped Oscillator.” <entropy.energy/scholar/node/driven-damped-oscillator>
[3] Nave, Rod. “Driven Oscillator.” Hyperphysics. (2017).
[4] Kerschen, G., M. Peeters, J.C. Golinval and A.F. Vakakis. “Nonlinear Normal Modes, Part I: A Useful Framework for the Structural Dynamicist.” *Mechanical Systems and Signal Processing* 23(1). (2009).
[5] Hanks, John. “Instruction Sheet for the PASCO Model CI-6689A.” PASCO. (1996).
[6] Tarnopolski, Mariusz. “On the fractal dimension of the Duffing attractor.” Rom. Rep. Phys. 66(3), 907-917 (2014).